Robotica (1999) volume 17, pp. 269–281. Printed in the United Kingdom © 1999 Cambridge University Press

Kinematic analysis and design of a six D.O.F. 3-PRPS in-parallel manipulator

J.H. Shim,* D.S. Kwon,** and H.S. Cho†

(Received in Final Form: October 26, 1998)

SUMMARY

This paper presents a kinematic analysis and design characteristics of an in-parallel manipulator developed for the probing task application that requires high precision, active compliance, and high control bandwidth. The developed manipulator is a class of six-degree-of-freedom in-parallel platforms with 3 PRPS (prismatic-revolute-prismatic-spherical joints) chain geometry. The main advantages of this manipulator, compared with the typical Stewart platform type, are the capability of pure rotation generation and the easy prediction of the moving platform motion. The purpose of this paper is to develop an efficient kinematic model which can be used for real-time control and to propose systematic methods to design the manipulator considering workspace, manipulability, resistivity, singularity, and the existence conditions of the forward kinematic solution. Particularly, we propose a new method for checking the singularity of the parallel manipulator using the translational and rotational resistivity measures. A series of simulation are carried out to show kinematic characteristics and performance of the manipulator mechanism. A prototype manipulator was built based on the kinematic analysis results.

KEYWORDS: Kinematic analysis; Kinematic design; In-parallel manipulator; PRPS joints, Real-time control.

1. INTRODUCTION

Recent development in the area of parallel manipulators has provided strong motivation for their versatile application. Obviously, parallel manipulators offer high structural stiffness and precise positioning accuracy over serial ones.

Many researchers have studied parallel manipulators, usually with the configuration known as a Stewart platform.[1–5] The Stewart platform was originally designed as an aircraft simulator.[1] Since then, various applications of the Stewart platform have been investigated such as a compliance device for assembly,[2] a force/torque sensor,[3] an active vibration isolator,[4] and a master controller mechanism for teleoperation.[5] But in general, the Stewart platform has some disadvantages that forward kinematics is too complex to solve in real-time and the prediction of the motion of each joint is not intuitive. Recently, Collins and Lang[5] have reported that the Stewart platform has at least 12 forward kinematic solutions.

Other configurations for parallel manipulators with six degree-of-freedom have also been proposed. Behi[6] developed a configuration with three legs where each leg consists of a PRPS chain. Hudgens and Tesar[7] investigated a device with six inextensible legs where each leg is driven by a four-bar mechanism mounted on the base platform. Alizade et al.[8] proposed a parallel manipulator which has three legs, mounted on moving sliders passing through a circular trajectory. Byun and Cho[9] presented a six degree-of-freedom 3-PPSP parallel manipulator which has three legs where each leg is driven by XY linear actuators. The mechanisms described in the above are partially parallel manipulators while the Stewart platform type mechanism is a fully parallel mechanism. Although these partially parallel mechanisms are developed to overcome some of disadvantages of the Stewart platform, previous works on these partially parallel manipulators have shown few industrial applications. Particularly, design of parallel manipulators with the PRPS joint structure for industrial applications has rarely reported in the open literature.

In the processes such as precision assembly, machining, and probing operation, robotic manipulators interact with the environment. Since the contact occurs in a very short period, limited control bandwidth of conventional robot controllers restricts their active force control. As one of the methods to solve the contact problem, concept of the macro/micro manipulator has been proposed.[10] A micro manipulator is attached to a macro conventional robot serially. The micro manipulator, generally a specialized device in the form of fingers or a wrist, is well adapted to active force control due to its low inertia. Some of the micro manipulator has parallel structures,[11] while most of their structures are based on the Stewart platform. The actuators of the manipulators are electrical rams or pneumatic actuators.

In the previous papers,[12,13] we developed a two degree-of-freedom probing mechanism for probing task such as in-circuit test of printed circuit boards. However, the mechanism shows a problem of slip motion where the probe contacts with steep surface of the contacted object. In

* Factory Automation Research Institute, Samsung Electronics Co., Ltd, 416 Maetan 3 Dong, Paldalgu, Suwon (Korea)
e-mail: jhshim@srtf.sec.samsung.co.kr
** Department of Mechanical Engineering, Korea Advanced Institute of Science and Technology, 373-1 Kusongdong, Yusonggu, Taejon (Korea)
e-mail: kwon@automation.kaist.ac.kr
† Department of Mechanical Engineering, Korea Advanced Institute of Science and Technology, 373-1 Kusongdong, Yusonggu, Taejon (Korea)
e-mail: hscho@lca.kaist.ac.kr

https://doi.org/10.1017/S0263574799001368 Published online by Cambridge University Press

addition, it was found that the limited degree-of-freedom of the probing device is not effective for contact force control.

To overcome these problems, we have studied new six degree-of-freedom probing mechanisms with a parallel structure. Among those studied, the proposed 3 PRPS parallel mechanism is found to generate two decoupled motions by moving the horizontal or vertical links.[14] One of the motions is composed of one degree of orientational freedom in the Z axis, and two degrees of translational freedom in the X and Y axes provided by the horizontal links of the mechanism. The other motion is two degrees of orientational freedom in the X and Y axes, and one degree of translational freedom in the Z axis provided by the vertical links of the mechanism. Particularly, since the vertical links can give constraint uniformly to the probe tip motion at the contact point, it is very effective in avoiding the slip motion, and to control the contact force at the probing task.

This paper presents a kinematic analysis of a 6 degree-of-freedom parallel manipulator, which we have developed for probing task that requires high control bandwidth, active compliance, and high precision. The developed manipulator belongs to a class of partially parallel platforms with 3 PRPS chains geometry whose design is based on the Behi mechanism.[8] Based on the concept of macro/micro manipulators, the parallel manipulator serves as a wrist of a macro manipulator. The manipulator consists of linear actuators by using the principle of Lorentz forcer, piezoelectric force sensors, and optical position sensors for real implementation,[13,14] while Behi introduced the conceptual design of the parallel manipulator with 3-PRPS chains. The main advantages of this manipulator, compared with the Stewart platform type, are the capability to produce pure rotation and to predict the motion of the moving platform intuitively. Also, this manipulator has simple kinematic characteristics compared with the Stewart platform. Therefore, controlling in real-time is possible due to a reduced computational burden.

Although the basic structure of the developed mechanism is similar to Behi platform, this paper emphasizes the following contents that have not been addressed by others: a simple kinematic model of the 3 PRPS type parallel manipulator which can be used for real-time control and a systematic approach to design the manipulator considering workspace, manipulability, resistivity, singularity, and the existence range of the forward kinematic solution.

2. INVERSE AND FORWARD KINEMATICS

The developed mechanism consists of a base plate, a top plate, three horizontal actuating links, and three vertical actuating links. The three horizontal links provide three degree-of-freedom, that are one degree of orientational freedom and two degrees of translational freedom. The three vertical links provide three degree-of-freedom, that are two degrees of orientational freedom and one degree of translational freedom.

The notation used to describe the kinematics of the proposed mechanism is shown in Figure 1. The fixed global coordinates called the base frame (X, Y, Z) is located at *O*, the center of the mass of the base plate with the X-axis

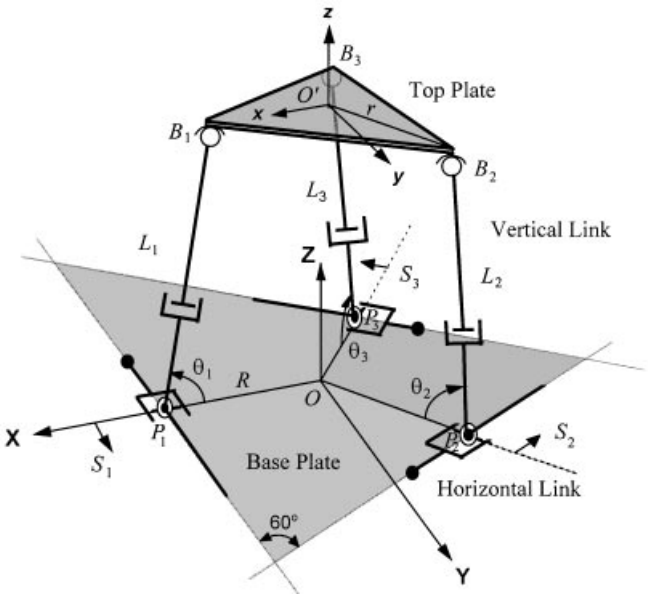

Fig. 1. Kinematic structure with coordinate assignment.

orthogonal to the first prismatic input axis of the first horizontal actuating link and the Z-axis normal to the base plate. Another reference coordinates, called the top frame (x, y, z), is located at O', the center of the mass of the top plate, the x-axis is pointing toward the ball joint B1, and the z-axis is normal to the top plate. The coordinates (x, y, z) with respect to the base frame (X, Y, Z) can be described by the vectors of the homogeneous transformation matrix $\begin{bmatrix} o \\ o' \end{bmatrix} T$:

$$\begin{bmatrix} o \\ o' \end{bmatrix} T = \begin{bmatrix} \vec{n}, \vec{o}, \vec{a}, \vec{p} \\ 0, 0, 0, 1 \end{bmatrix} = \begin{bmatrix} n_1 & o_1 & a_1 & X_c \\ n_2 & o_2 & a_2 & Y_c \\ n_3 & o_3 & a_3 & Z_c \\ 0 & 0 & 0 & 1 \end{bmatrix} \quad (1)$$

where $(\vec{n}, \vec{o}, \vec{a})$ and $(X_c, Y_c, Zc)^{\mathrm{T}}$ describe the orientation vector and the position of the top plate center with respect to the base frame (X, Y, Z), respectively. The top plate is connected to the vertical links with ball joints B_i which are equally spaced at 120 degrees and at a radius r from the center of the top plate as shown in Figure 2(a). The other ends of the vertical links are connected to the horizontal links through equally spaced pin joints P_i at a radius R from the center of the base plate. By varying the link lengths, the top plate can be manipulated with respect to the base plate. The Cartesian position vector $\vec{B}_i$ of the ball joint with respect to the base frame (X, Y, Z) can be expressed as

$$\vec{B}_i = \begin{bmatrix} o \\ o' \end{bmatrix} T \vec{P}_i \quad (2)$$

where $\vec{P}_i$ is the position vector of the pin joint with respect to the top frame (x, y, z).

The inverse kinematics problem can be briefly stated as: for a given position and orientation of the top platform,

https://doi.org/10.1017/S0263574799001368 Published online by Cambridge University Press

compute the actuating length of each link. The links P_1B_1, P_2B_2, *and* P_3B_3 are constrained by the pin joints to move in the plates, $Y = S_1$, $Y = -\sqrt{3}X - 2S_2$, $Y = \sqrt{3}X - 2S_3$, respectively, where S_i is the actuating length of the ith horizontal link for i = 1, 2, 3. From the constraint equation, we can obtain S_i as follows:

$$S_1 = n_2 r + Y_c$$

$$S_2 = \frac{\sqrt{3}}{4} n_1 r + \frac{1}{4} n_2 r - \frac{3}{4} o_1 r - \frac{\sqrt{3}}{4} o_2 r - \frac{\sqrt{3}}{2} X_c - \frac{1}{2} Y_c \quad (3)$$

$$S_3 = -\frac{\sqrt{3}}{4} n_1 r + \frac{1}{4} n_2 r - \frac{3}{4} o_1 r + \frac{\sqrt{3}}{4} o_2 r + \frac{\sqrt{3}}{2} X_c - \frac{1}{2} Y_c.$$

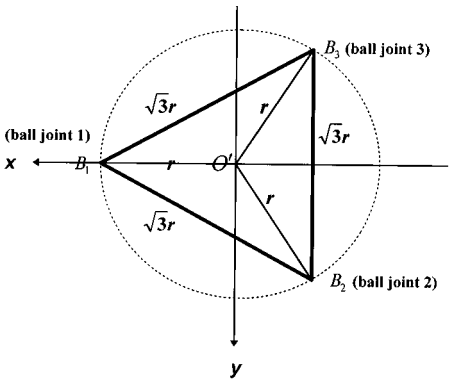

(a) The shape of the top plate projected on the ***x-y*** plane

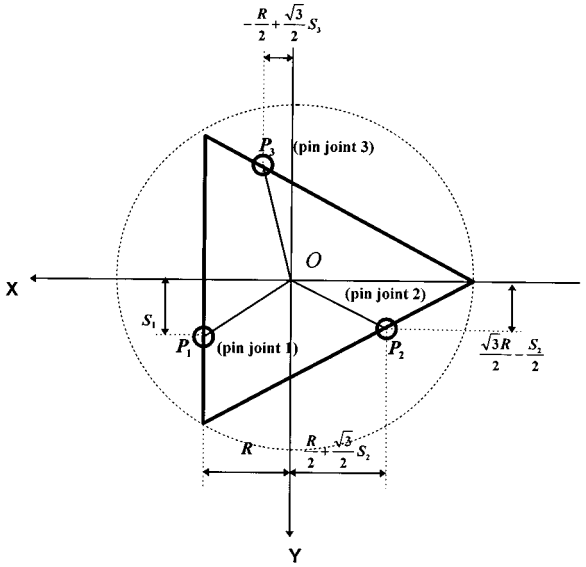

(b) The shape of the base plate projected on the **X-Y** plane

Fig. 2. The geometry of the top plate and the base plate of the 3-PRPS parallel manipulator.

Then, the lengths of the vertical links L_i can be obtained from the following vector analysis:

$$\vec{OO'} + \vec{O'B_i} = \vec{OP_i} + \vec{P_iB_i} \text{ for } i = 1, 2, 3. \quad (4)$$

From the above (4), the following solution of the inverse kinematics is obtained:

$$L_1^2 = X_C^2 + Y_C^2 + Z_C^2 + r^2 + R^2 + S_1^2 - 2RX_C^X - 2S_1Y_C + 2rn_1(X_C - R) + 2rn_2(Y_C - S_1) + 2rn_3Z_C$$

$$L_2^2 = X_C^2 + Y_C^2 + Z_C^2 + r^2 + R^2 + S_2^2 + RX_C - \sqrt{3}RY_C + \sqrt{3}S_2X_C + S_2Y_C + (X_C + \frac{1}{2}R + \frac{\sqrt{3}}{2}S_2)(\sqrt{3}o_1 - n_1)r + (Y_C - \frac{\sqrt{3}}{2}R + \frac{1}{2}S_2)(\sqrt{3}o_2 - n_2)r + (\sqrt{3}o_3 - n_3)rZ_C$$

$$L_3^2 = X_C^2 + Y_C^2 + Z_C^2 + r^2 + R^2 + S_3^2 + RX_C + \sqrt{3}RY_C - \sqrt{3}S_3X_C + S_3Y_C - (X_C + \frac{1}{2}R - \frac{\sqrt{3}}{2}S_3)(\sqrt{3}O_1 + n_1)r - (Y_C + \frac{\sqrt{3}}{2}R + \frac{r}{2}S_3)(\sqrt{3}o_2 + n_2)r - (\sqrt{3}O_3 + n_3)rZ_C. \quad (5)$$

If the position of the top plate is given, the solutions of the inverse kinematics are uniquely determined as shown in (2) and (4).

The forward kinematics problem can be stated as: for given actuating lengths of the extensible links, compute the position (X_C, Y_C, Z_C) and orientation vector $\vec{n}$, $\vec{o}$, $\vec{a}$ of the top platform. The angles θ_i are defined to be the angles between the base platform and the vertical links P_iB_i (for i=1, 2, 3). Since the distance between any two adjacent ball joints is $\sqrt{3}r$, the following vector relations can be obtained by:

$$\vec{OP_i} + \vec{P_iB_i} + \vec{B_iB_j} = \vec{OP_j} + \vec{P_jB_j} \ (for\ i = 1, 2, 3, j = 2, 3, 1) \quad (6)$$

$$\| \vec{B_iB_j} \|^2 = \left(\sqrt{3}r \right)^2 = \| \vec{OP_j} + \vec{P_jB_j} - \vec{OP_i} - \vec{P_iB_i} \|^2. \quad (7)$$

From the above (7), the implicit relationships between θ_i and six lengths of the extensible links L_i, S_i are described by:

$$f_1(\theta_1, \theta_2) = L_1^2 + L_2^2 + L_1L_2\cos\theta_1\cos\theta_2 - 2L_1L_2\sin\theta_1 \sin\theta_2 - L_1\cos\theta_1(3R + \sqrt{3}S_2) + L_2\cos\theta_2(-3R + \sqrt{3}S_1) + 3R^2 - 3r^2 + S_1^2 + S_2^2 + S_1S_2 + R(-\sqrt{3}S_1 + \sqrt{3}S_2) = 0$$

$$f_2(\theta_2, \theta_3) = L_2^2 + L_3^2 + L_2L_3\cos\theta_2\cos\theta_3 - 2L_2L_3\sin\theta_2 \sin\theta_3 - L_2\cos\theta_2(3R + \sqrt{3}S_3) + L_3\cos\theta_3(-3R + \sqrt{3}S_3) + 3R^2 - 3r^2 + S_2^2 + S_3^2 + S_2S_3 + R(-\sqrt{3}S_2 + \sqrt{3}S_3) = 0$$

$$f_3(\theta_1, \theta_3) = L_1^2 + L_3^2 + L_1L_3\cos\theta_1\cos\theta_3 - 2L_1L_3\sin\theta_1 \sin\theta_3 - L_1\cos\theta_1(3R - \sqrt{3}S_3) + L_3\cos\theta_3(3R + \sqrt{3}S_1) + 3R^2 - 3r^2 + S_1^2 + S_3^2 + S_1S_3 + R(\sqrt{3}S_1 - \sqrt{3}S_3) = 0. \quad (8)$$

https://doi.org/10.1017/S0263574799001368 Published online by Cambridge University Press

We thus have three nonlinear equations for three unknowns θ_i. Their solutions can be obtained numerically.

To control the manipulator in real-time without additional sensor for sensing the position and orientation of the end effector installed at the top plate, it is very important to compute θ_i fast by using L_i and S_i sensed from the position sensors of the links. In this paper, the Newton-Raphson method[15] is used to solve the nonlinear equations. Since the initial value of θ_i is critical to the calculation time of the Newton-Raphson method, the initial value has to be guaranteed to meet the required computing time constraints within the workspace. Once the initial values are chosen, then, the position vector $\vec{B}_i$ can be obtained from the calculated θ_i and the geometry of Figure 2(b) as follows:

$$\vec{B}_1=[X_{B1}\ Y_{B1}\ Z_{B1}]^{\mathrm{T}}=[R-L_1\cos\theta_1 \quad S_1 \quad L_1\sin\theta_1]^{\mathrm{T}}$$

$$\vec{B}_2=[X_{B2}\ Y_{B2}\ Z_{B2}]^{\mathrm{T}}$$

$$=\left[-\frac{R}{2}-\frac{\sqrt{3}}{2}S_2+\frac{1}{2}L_2\cos\theta_2 \quad \frac{\sqrt{3}}{2}\mathrm{R} \right.$$

$$\left.-\frac{1}{2}\mathrm{S}_2-\frac{\sqrt{3}}{2}\mathrm{L}_2\cos\theta_2 \quad L_2\sin\theta_2\right]^{\mathrm{T}}$$

$$\vec{B}_3=[X_{B3}\ Y_{B3}\ Z_{B3}]^{\mathrm{T}}$$

$$=\left[-\frac{R}{2}+\frac{\sqrt{3}}{2}S_3+\frac{1}{2}L_3\cos\theta_3 \quad -\frac{\sqrt{3}}{2}\mathrm{R} \right.$$

$$\left.-\frac{1}{2}\mathrm{S}_3+\frac{\sqrt{3}}{2}\mathrm{L}_3\cos\theta_3 \quad L_3\sin\theta_3\right]^{\mathrm{T}} \qquad (9)$$

Since the ball joints are placed at the vertices of an equilateral triangle, (X_C, Y_C, Z_C) can be expressed by

$$X_C=\frac{1}{3}\sum_{i=1}^{3}X_{Bi}$$

$$Y_C=\frac{1}{3}\sum_{i=1}^{3}Y_{Bi}$$

$$Z_C=\frac{1}{3}\sum_{i=1}^{3}Z_{Bi}\,. \qquad (10)$$

Then, the orientation vectors can be ($\vec{n}$, $\vec{o}$, $\vec{a}$) calculated using (2) and (9).

From (6), we know that multiple solutions of the angles θ_i exist for a given set of link lengths. In other words, there are multiple possible configurations of the manipulator for a specific set of link displacements.

To verify the correctness of the derived kinematic model, a series of simulations were carried out as follows: First, we obtain a sphere within the reachable workspace of the proposed manipulator and divide the surface of the sphere to have equal dividing intervals as shown in Figure 3. Secondly, by using the inverse kinematics, the lengths of the vertical and the horizontal links are obtained corresponding to the position and orientation of the center of the top platform as shown in Figures 4(a) and(b). Thirdly, forward kinematic solutions are calculated from the obtained inverse kinematic solutions. Figure 5 shows the result of the forward kinematics. The correctness of the derived kinematic model is checked by comparing the deviation between Figure 3 and Figure 5. They absolutely matched each other.

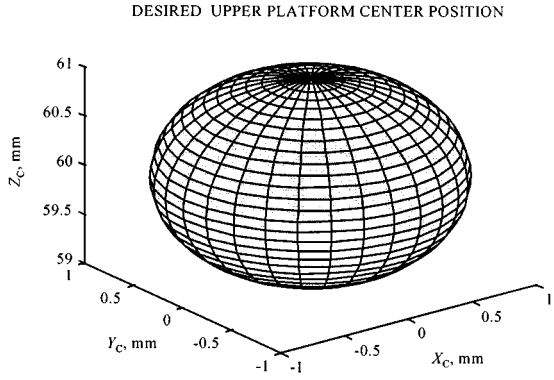

Fig. 3. The desired workspace for simulation.

3. EXISTENCE OF THE FORWARD KINEMATIC SOLUTION

Since a parallel manipulator consists of closed chains, there are kinematic constraints that restrict the motion of the links of the manipulator. Some solutions of the forward kinematics are not realizable according to combinations of the link displacements. In this section, we introduce conditions for checking the existence of the forward kinematics solutions for the proposed in-parallel manipulator.

The kinematic constraints that restrict the motion of the links are described by (8). From the constraints, we determine the critical points that has an unique kinematic solution in the whole workspace. A set of equations for obtaining the points at which the rates of variation of f_1, f_2, and f_3 are zero can be derived by:

$$\frac{\partial f_1}{\partial\theta_1}+\frac{\partial f_1}{\partial\theta_2}=0$$

$$\frac{\partial f_2}{\partial\theta_2}+\frac{\partial f_2}{\partial\theta_3}=0 \qquad (11)$$

$$\frac{\partial f_3}{\partial\theta_1}+\frac{\partial f_3}{\partial\theta_3}=0$$

The solution of above non-linear equation (11) is given by:

$$\theta_1=\theta_2=\theta_3=\pm n\pi \quad \text{for } n=0,\ 1,\ 2,\ \ldots \qquad (12)$$

Let us denote the ratio of the top plate and the base plate size ρ as

https://doi.org/10.1017/S0263574799001368 Published online by Cambridge University Press

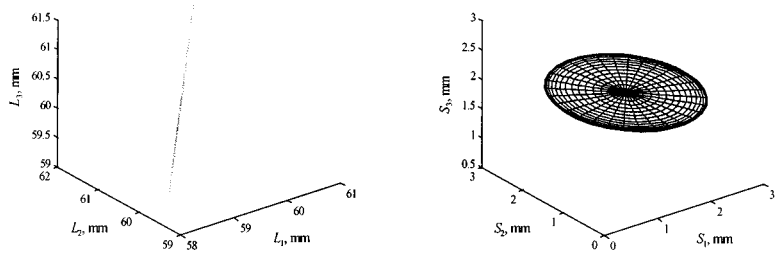

(a) Variation of the vertival links (b) Variation of the horizontal links

Fig. 4. Solutions of the inverse kinematics.

$$\rho = \frac{r}{R} \tag{13}$$

Considering the configuration of the proposed mechanism by varying ρ, we know that the solutions simultaneously satisfying (11) indicates the following two cases only:

$$\theta_1 = \theta_2 = \theta_3 = 0 \quad \text{if } \rho = \frac{r}{R} \le 1,$$

$$\theta_1 = \theta_2 = \theta_3 = \pi \quad \text{if } \rho = \frac{r}{R} > 1. \tag{14}$$

The above two cases represent the configurations of the mechanism whose forward kinematic solution exists uniquely. In other words, the conditions of (14) represent critical points that has unique kinematic solution in whole workspace of the manipulator. Therefore, a general existence condition of the forward kinematic solution including the critical points of (14) can be obtained by substituting (14) into (8):

$$f_i(0,0) \le 0 \quad \text{if } \rho = \frac{r}{R} \le 1,$$

$$f_i(\pi,\pi) \le 0 \quad \text{if } \rho = \frac{r}{R} > 1, \quad \text{for } i = 1,2,3. \tag{15}$$

Let us consider a special case in which the lengths of three vertical links and three horizontal links are identical that is: $L_1 = L_2 = L_3 = L$, $S_1 = S_2 = S_3 = S$. From (8), the solutions satisfying the inequality of (14) are given in the following forms:

$$\frac{L}{r} \ge \frac{R}{r} - \sqrt{1 - \left(\frac{S}{r}\right)^2} \text{ if } \rho = \frac{r}{R} \le 1 \quad \left(-1 \le \frac{S}{r} \le 1\right),$$

$$\frac{L}{r} \ge \left| -\frac{\mathrm{R}}{\mathrm{r}} + \sqrt{1 - \left(\frac{S}{r}\right)^2} \right| \text{ if } \rho = \frac{r}{R} > 1 \ \left(-1 \le \frac{S}{r} \le 1\right) \tag{16}$$

Figure 6 shows the existence range of the forward kinematic solution satisfying the inequality of (16). For each ρ, (16) means that the kinematic solutions exist at the upper zones of the obtained curves.

Generally, the forward kinematics of parallel manipulators doesn't have a unique solution, but multiple solutions. The simulations for the forward kinematics of the proposed manipulator result in eight distinct solutions according to the initially guessed θ_i. Figure 7 shows the results of (16) at the conditions of which $R = r = 50$ [mm], $L_1 = L_2 = L_3 = 100$[mm], $S_1 = S_2 = S_3 = 0$, and $-180° \le \theta_i \le 180°$ for $i = 1, 2, 3$. We know that the sets of (θ_1, θ_2), (θ_2, θ_3), and (θ_3, θ_1) form a certain shape of band satisfying $f_i = 0$ of (8) respectively. These shapes mean that there exist multiple solutions for the forward kinematics of the proposed mechanism.

A series of numerical analysis represent the existence of the eight distinct forward kinematic solutions as shown in Figure 8.

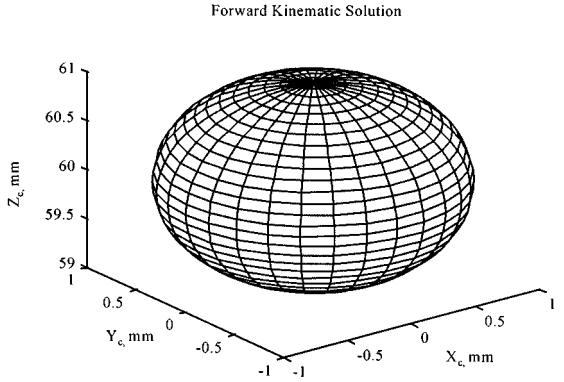

Fig. 5. The workspace obtained by the solution of the forward kinematics.

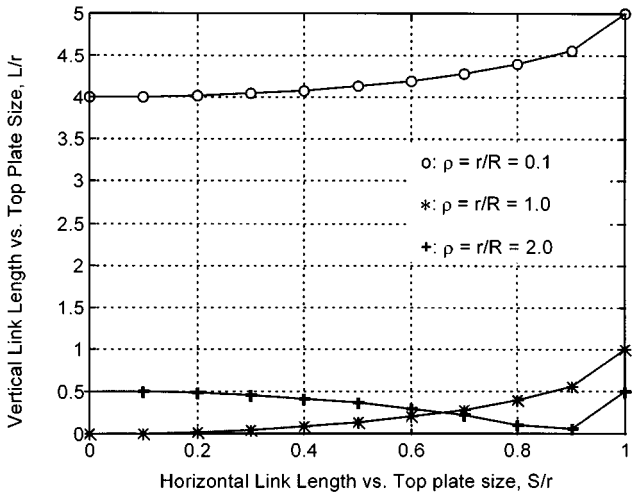

Fig. 6. Existence rabge of the forward kinematic solution.

https://doi.org/10.1017/S0263574799001368 Published online by Cambridge University Press

As noted earlier, fast computation of kinematics is very important to control a parallel manipulator in real-time. In this paper, we developed the kinematic model on a personal computer with a 80486-DX2 66MHz CPU. The inverse and forward kinematics take approximately 2 miliseconds. These results are fast enough to allow us to implement a real-time control of the proposed manipulator with a good frequency response.

4. WORK SPACE ANALYSIS

Generally, the work space of the Stewart platform type manipulator forms a certain type of an umbrella whose sectional area is changing according to the height.[16] These characteristics may restrict the possible applications of the manipulator for various tasks. The proposed manipulator has an uniform workspace without variation of the sectional area, although its height varies. The workspace always forms a shape of a hexagonal pole irrespective of the variation of the ratio ρ. Figure 9 compares the workspaces of the two manipulators with $R=50$ [mm], $\rho=1$, $0 \le L_i \le 1.2R$, and $-0.1R \le S_i \le 0.1R$ for $i=1, 2, 3$.

The relationship between ρ and the volume of the workspace by varying the actuating lengths of the links is shown in Figure 10. Clearly, as ρ decreases, larger workspace is obtained.

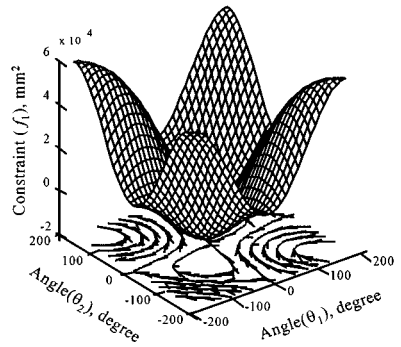

(a) $f_1(\theta_1, \theta_2) = 0$

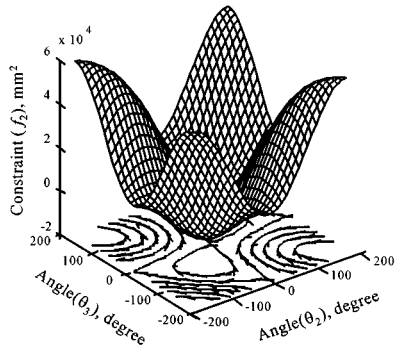

(b) $f_2(\theta_2, \theta_3) = 0$

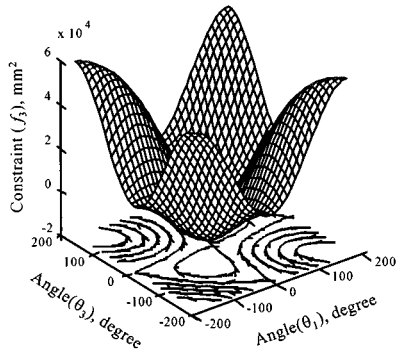

(c) $f_3(\theta_3, \theta_1) = 0$

Fig. 7. Graphs of multiple existence of the forward kinematic solution.

5. MANIPULABILITY AND RESISTIVITY

Manipulability measure $\boldsymbol{w}$ was proposed to measure quantitatively the ability of changing the end-effector position and orientation from the view point of the kinematics.[17] In a serial manipulator, the relation between the joint velocity $\dot{q}$ and the velocity vector $\boldsymbol{\nu}$ corresponding to the position and/or orientation of the end effector is

$$\nu = J(q)\dot{q} \tag{17}$$

where q is the joint variable of the manipulator and J is the Jacobian matrix. The manipulability measure $\boldsymbol{w}$ for the serial manipulator configuration q is given by

$$\boldsymbol{w} = \sqrt{\det(J\,J^T)} \tag{18}$$

For a parallel manipulator, let $Q=[Q_1, \ldots, Q_6]^{\mathrm{T}}$ be a displacement vector of six actuators and $C=[X_C, T_C, Z_C, \alpha, \beta, \gamma]^{\mathrm{T}}$ be a generalized coordinate vector representing the position/orientation of the top platform. The Jacobian matrix J relates the joint velocities $\dot{Q}$ to the Cartesian and angular velocities of the end-effector $\dot{C}$ as:

$$\dot{Q} = J(C)\,\dot{C} \tag{19}$$

Since Jacobian matrix J of parallel manipulators is derived from the inverse kinematics, it is the inverse one of the serial ones. The Jacobian matrix J describing the relationship between the end-effector force F and the joint torque τ for the parallel manipulator is given as follows:

$$F = \begin{bmatrix} f_c \\ m_c \end{bmatrix} = J^T \tau \tag{20}$$

where f_c, m_c are the decoupled force and moment of the end-effector, respectively.

Since the proposed parallel manipulator has no redundant degree-of-freedom, the manipulability measure $\boldsymbol{w}$ is represented as follows:

$$\boldsymbol{w} = \left| \det(J^{-1}) \right| \tag{21}$$

The concept of resistivity measure, $\boldsymbol{w}_{\mathrm{R}}$, of robot manipulators was suggested as a quantitative measure of their

https://doi.org/10.1017/S0263574799001368 Published online by Cambridge University Press

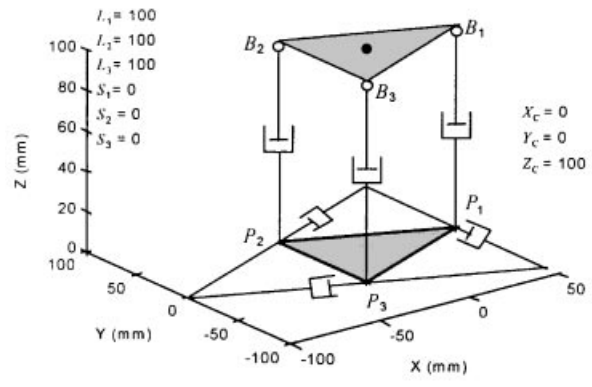

(a) $\theta_1 = 90°$, $\theta_2 = 90°$, $\theta_3 = 90°$

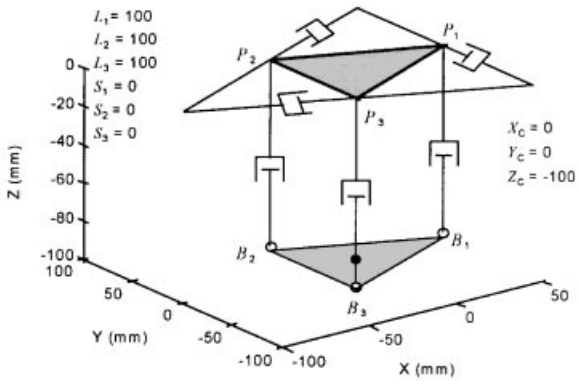

(b) $\theta_1 = -90°$, $\theta_2 = -90°$, $\theta_3 = -90°$

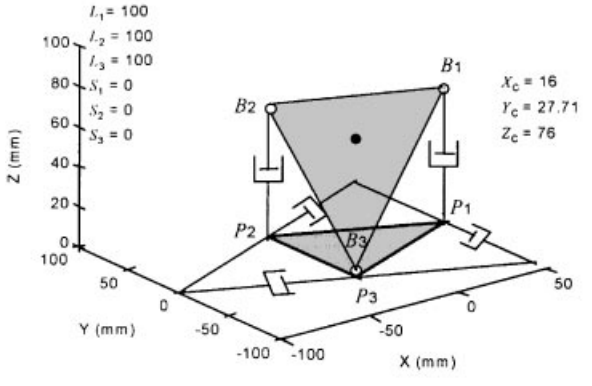

(c) $\theta_1 = 90°$, $\theta_2 = 90°$, $\theta_3 = 16.2°$

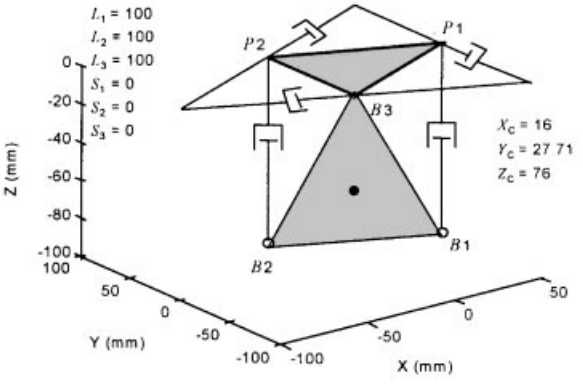

(d) $\theta_1 = -90°$, $\theta_2 = -90°$, $\theta_3 = -16.2°$

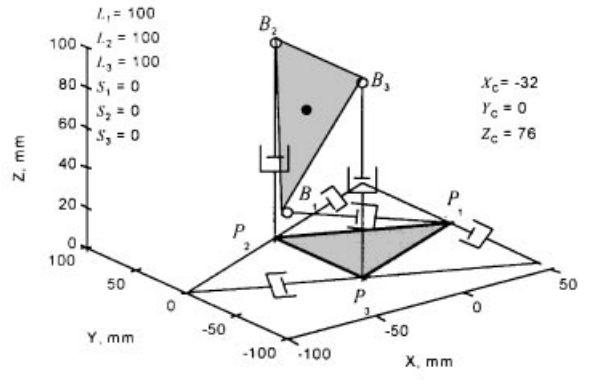

(e) $\theta_1 = 16.2°$, $\theta_2 = 90°$, $\theta_3 = 90°$

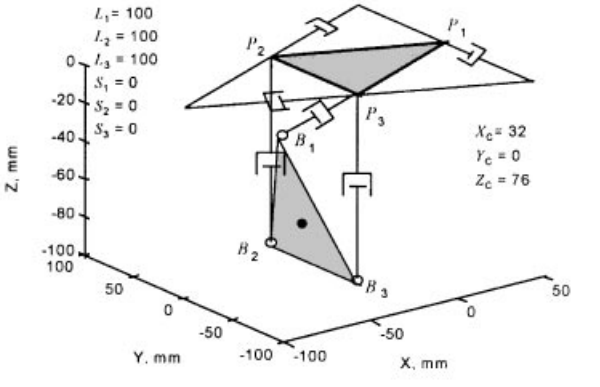

(f) $\theta_1 = -16.2°$, $\theta_2 = -90°$, $\theta_3 = -90°$

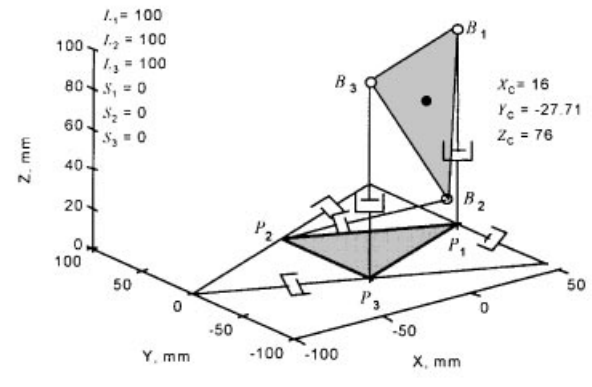

(g) $\theta_1 = 90°$, $\theta_2 = 16.2°$, $\theta_3 = 90°$

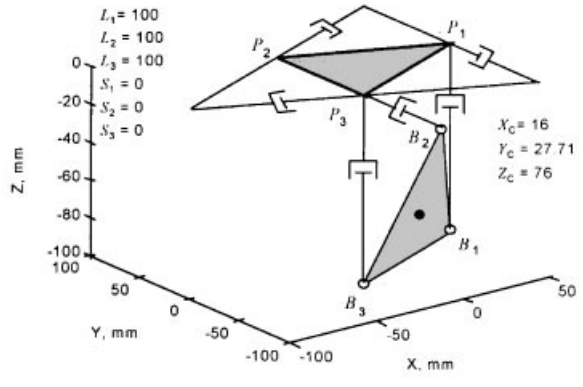

(h) $\theta_1 = -90°$, $\theta_2 = -16.26°$, $\theta_3 = -90°$

Fig. 8. Configurations of the eight distinct forward kinematic solutions.

https://doi.org/10.1017/S0263574799001368 Published online by Cambridge University Press

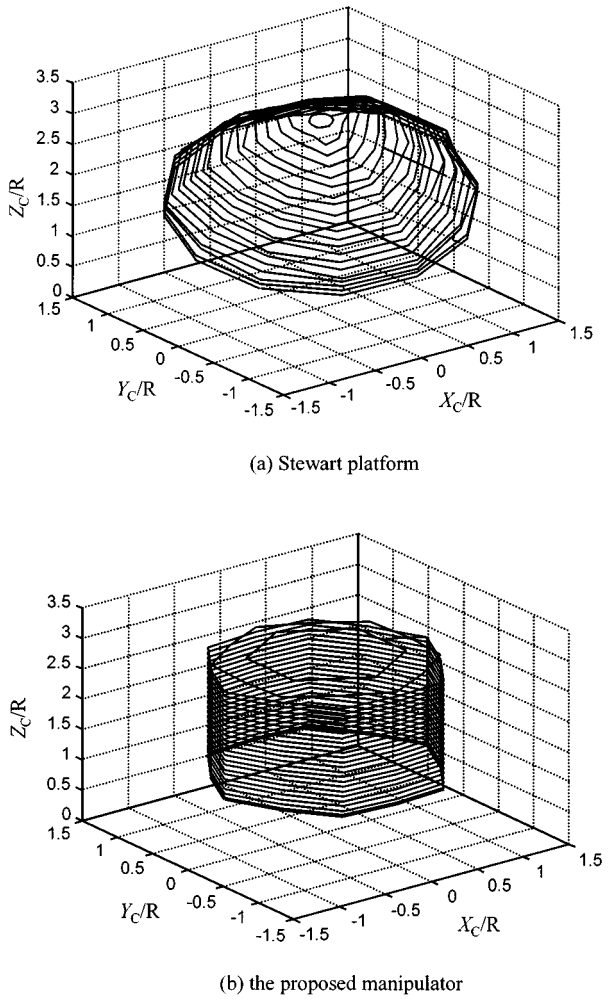

(a) Stewart platform

(b) the proposed manipulator

Fig. 9. Comparison of the workspace for the Stewart platform and the proposed manipulator in case of $\rho = 1$.

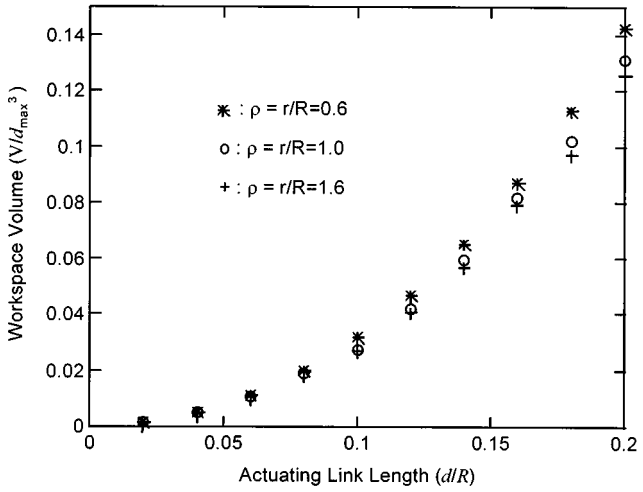

Fig. 10. Variation of workspace volume by varying the actuating lengths of the links d and the $\rho(d_{max}$ = maximum actuating link length).

ability in resisting the externally applied forces.[17] The resistivity measure for the proposed non-redundant parallel manipulator can be written as follows:

$$w_R = \frac{1}{w} = \frac{1}{|\det(J^{-1})|} \tag{23}$$

Since the manipulability and resistivity are functions of the Jacobian, their values are changed according to configurations of the manipulator. For a configuration with $X_C = 0$, $Y_C = 0$, $Z_C = 60$ [mm] and the orientation angles of the top platform $\alpha = 0°$, $\beta = 5°$, $\gamma = 0°$ where they are expressed in terms of Euler angles, the simulation results by varying ρ are shown in Figure 11.

It is found in Figure 11 that ρ less than 1 results in rapid increase of the manipulability, while ρ greater than 1 results in monotonously decreasing magnitude of the manipulability. The resistivity shows the reverse trends compared with the case of the manipulability. Therefore, the manipulator is recommended to be designed with $\rho < 1$ for good manipulation. But for large stiffness, it must be designed with $\rho > 1$.

6. SINGULARITY ANALYSIS

Parallel manipulators have certain singular configurations at which it is impossible to move the top platform no matter which joint rates are selected. From (19), the inverse Jacobian matrix J^{-1} relates the joint velocities $\dot{Q}$ to the Cartesian and angular velocities of the end-effector $\dot{C}$ as:

$$\dot{C} = J^{-1}(C)\dot{Q} \tag{24}$$

If the determinant of J is equal to zero in a given configuration C_O, the velocities of the end-effector become infinity, and the manipulator is uncontrollable. We call this C_O a singular configuration. Considering the singular configuration from the view point of the end-effector force F and the joint torque τ, we see that at the configuration small changes of F can easily destroy the balance of the structural rigidity. In other words, in order to maintain the rigidity infinite joint torque τ is required as shown in (20). Conventionally, singular configurations of parallel manip-

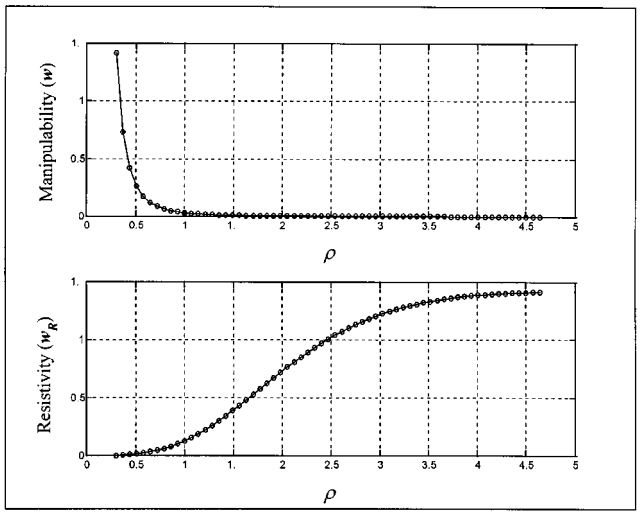

Fig. 11. Manipulability and resistivity with respect to ρ.

https://doi.org/10.1017/S0263574799001368 Published online by Cambridge University Press

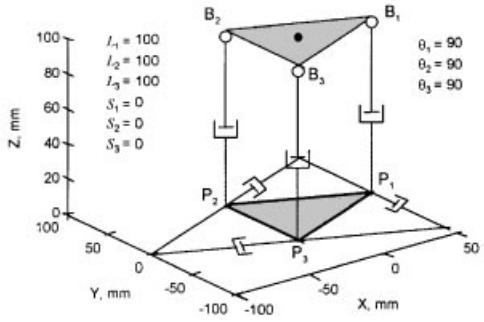

(a)

$X_C = 0$, $Y_C = 0$, $Z_C = 100$, $\alpha = 0°$, $\beta = 0°$, $\gamma = 0°$

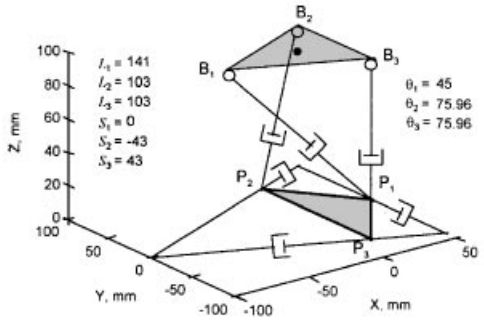

(b)

$X_C = 0$, $Y_C = 0$, $Z_C = 100$, $\alpha = 0°$, $\beta = 180°$, $\gamma = 0°$

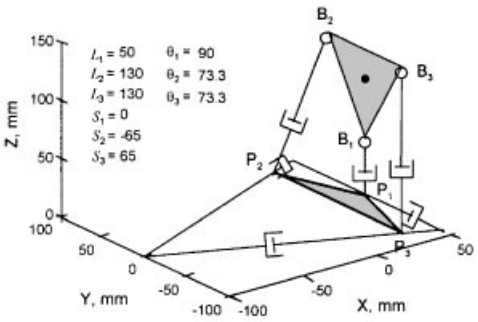

(c)

$X_C = 50$, $Y_C = 0$, $Z_C = 100$, $\alpha = 0°$, $\beta = 90°$, $\gamma = 0°$

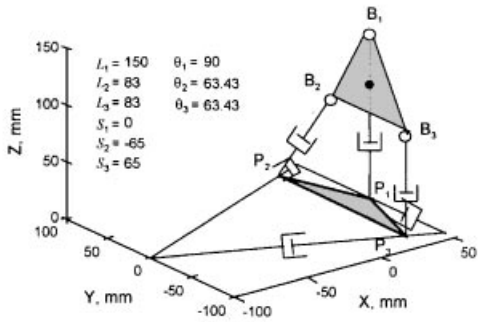

(d)

$X_C = 50$, $Y_C = 0$, $Z_C = 100$, $\alpha = 0°$, $\beta = -90°$, $\gamma = 0°$

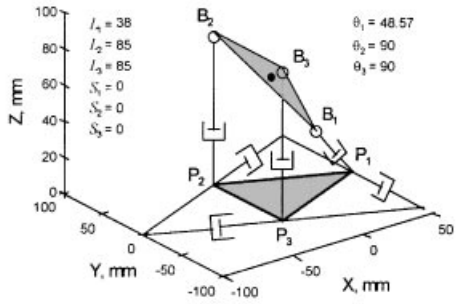

(e)

$X_C = -8.5$, $Y_C = 0$, $Z_C = 66.2$ $\alpha = 0°$, $\beta = 48.5°$, $\gamma = 0°$

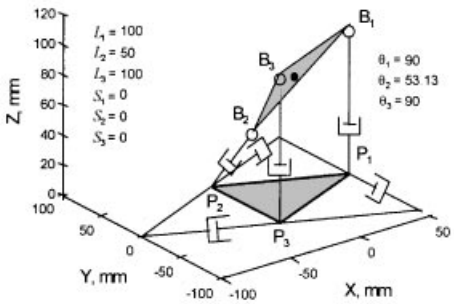

(f)

$X_C = 5$, $Y_C = -8.6$, $Z_C = 80$, $\alpha = 120°$, $\beta = -53.1°$, $\gamma = -120°$

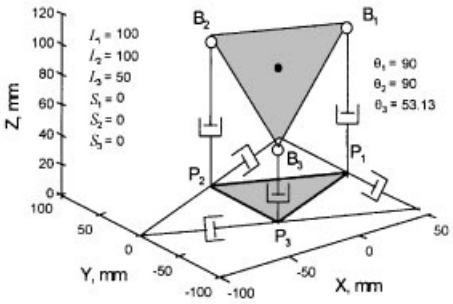

(g)

$X_C = 5$, $Y_C = 8.6$, $Z_C = 80$, $\alpha = -120°$, $\beta = 53.1°$, $\gamma = 120°$

Fig. 12. Seven singular configurations of the proposed manipulator.

https://doi.org/10.1017/S0263574799001368 Published online by Cambridge University Press

ulators can be described by checking the determinant of Jacobian matrix. Mac-Callion and Pham[18] used a numerical deflation method to find out all roots of the determinant. They found up to nine roots to this determinant, all outside the range of the links length. Fichter[19] described sinular configurations that is obtained when one rotates the mobile plate aroung z axis with an angle of $\pm \frac{\pi}{2}$. This configuration was obtained by investigating the roots of the determinant of Jacobian matrix. Gosselin and Angeles[20] described a classification of singularity of closed-loop kinematic chains in three groups, which is based on the properties of the Jacobian matrix. Practically, however, these conventional approaches introduced in the above are difficult to use for the investigation of the singularity because the Jacobian matrix of most parallel manipulators is highly nonlinear and complex.

These problems inherent to parallel manipulators have led some researchers to explore geometric methods.[21–22] Merlet[21] proposed a singularity analysis method based on Grassman line geometry.[23] In this method, a singular configuration is obtained when the parallel manipulator satisfies several geometric rules describing the geometric lines associated to the robot links. It appears that this method can be applied for a specific parallel manipulator, not for the general parallel manipulators.

Manipulability measure $\boldsymbol{w}$ has been used to analyze the singular configuration for serial robots.[15] In this paper, we apply this measure for the singularity analysis of the 3-PRPS parallel manipulator. Generally, the parallel manipulator has a singular configuration at the position and orientation of $\boldsymbol{w}=\infty$. However, it is not easy to accurately obtain the physical meaning of the singular configuration, as the motion of the end-effector of parallel manipulators is generated by highly coupled link motions. Sometimes, various tasks of robot make us to consider the robot motion decoupled into translation and rotation. For example, probing is accomplished mostly by translational motion, while micro-surgery is dominated by rotational motion.[24] Therefore, in order to understand the singularity more intuitively, we think that the motion of the parallel manipulator should be analyzed by being separated into translational and rotational motions in the Cartesian coordinates. Arai and Sheridan[25] proposed the singular value decomposition of the Jacobian to analyze how to generate forces and moments at the end-effector. The Jacobian was partitioned into two matrices, one corresponding to force and the other to moment. They also discussed the singularity of the Stewart platform by using this analysis method. In this paper, we adopt the translationalability and the rotationalability[26] to analyze the singular configurations of the 3-PRPS parallel manipulator. The method for checking singularity adopted here is similar to that proposed by Arai and Sheridan. Translationalability was proposed to evaluate the ability of a manipulator which can generate translational forces of its top platform. The Jacobian matrix J can be decomposed as follows:

$$F=\begin{bmatrix} f_c \\ m_c \end{bmatrix}=J^T\tau=\begin{bmatrix} J_T^{\mathrm{T}} \\ J_T^{\mathrm{T}} \end{bmatrix}\tau \tag{25}$$

where $J_T(\in \mathbf{R}^{6\times 3})$, $J_R(\in \mathbf{R}^{6\times 3})$, are the submatrices of J which denote the translational and rotational motions, respectively. If only translational motion of the top plate is generated without any rotational motion by the link forces, the following relations are obtained from (25):

$$f_c=J_T^T\tau\neq 0, \quad f_c \in \Re\,(J_T^T)$$
$$\tau_c=J_R^T\,\tau=0 \tag{26}$$

Table I. Geometric conditions of the seven singular configurations

Type	α	β	γ	X_C	Y_C	Z_C
a	0	$\pm n\pi$*	0	arbitrary	arbitrary	arbitrary
b	0	$\pm(n+1)\pi$	0	arbitrary	arbitrary	arbitrary
c	0	$+\frac{n\pi}{2}$	0	R	arbitrary	
d	0	$+\frac{(n+1)\pi}{2}$	0	R	0	arbitrary
e	0	$\tan^{-1}\frac{Z_C}{R-X_C}$	0	arbitrary	arbitrary	arbitrary
f	$\frac{2\pi}{3}$	$\tan^{-1}\left(\frac{Z_C}{R+k}\right)$	$-\frac{2\pi}{3}$	$\lvert k\sin\alpha\rvert$**	$-\lvert k\sin\alpha\rvert$	arbitrary
g	$-\frac{2\pi}{3}$	$\tan^{-1}\left(\frac{Z_C}{R+k}\right)$	$\frac{2\pi}{3}$	$\lvert k\sin\alpha\rvert$	$-\lvert k\sin\alpha\rvert$	arbitrary

* n = 1, 3, 5, . . .
** $k > 0$

https://doi.org/10.1017/S0263574799001368 Published online by Cambridge University Press

where $\Re\,(J_T^T)$ denotes the range of J_T^T. Now, we consider the set of end-effector forces f_c which are realizable for the joint forces τ such that the Euclidean norm of τ satisfies,

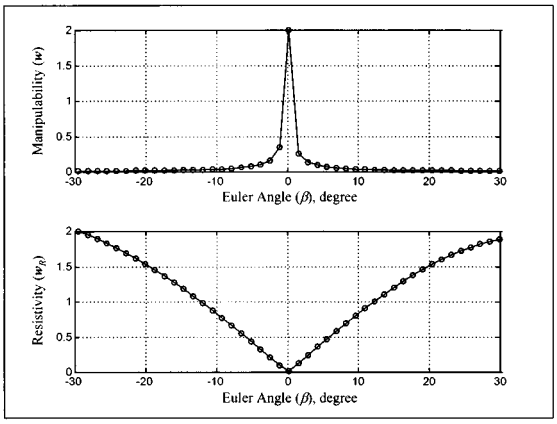

(a) w and w_R

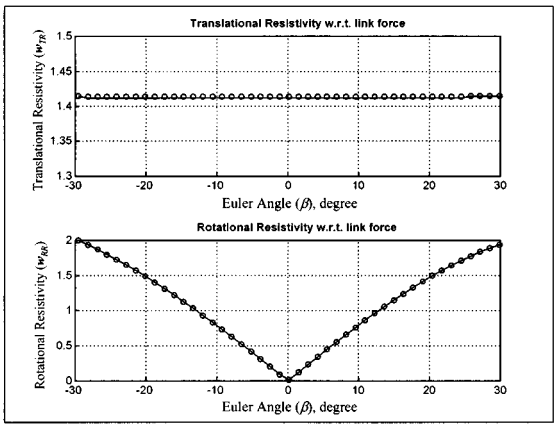

(a) w_{TR} and w_{RR}

Fig. 13. Manipulability, resistivity, translational resistivity, and rotational resistivity at the configuration with $\alpha=\gamma=0°$.

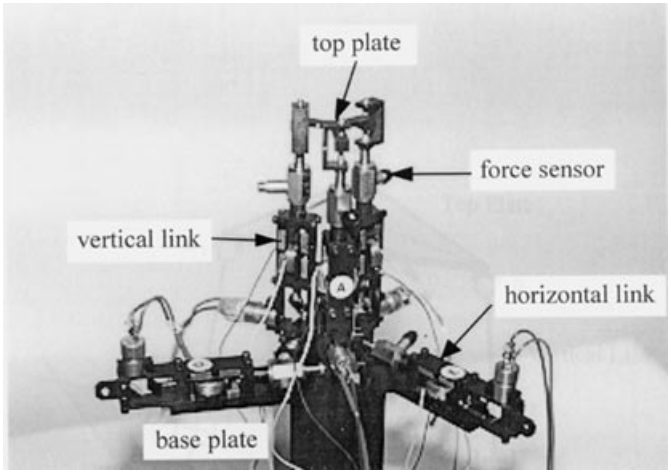

Fig. 14. A photograph of the proposed parallel manipulator.

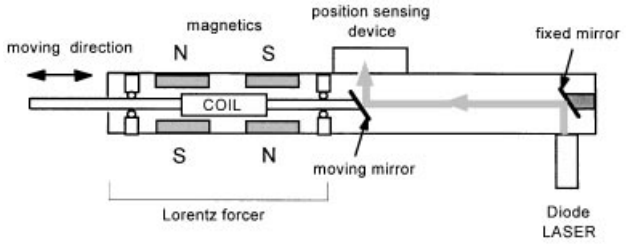

Fig. 15. The joint actuator with an optical sensing mechanism.

$$\| \tau \|^2=(\tau_1^2+\tau_2^2+ \ldots +\tau_6^2)\leq 1. \tag{27}$$

From (25) and (26), we have

$$\tau^T\tau=f_c^T(J_T)^+(J_T^T)^+f_c \tag{28}$$

where J_T^+ is the pseudo-inverse matrix of J_T. Equation (28) means that the resulting forces of the top plate forms an ellipsoid in the three-dimensional Euclidean space, whose space lies in the directions of the eigenvectors of the matrix $(J_T)^+(J_T^T)^+$. The volume of the ellipsoid represents the magnitude of the translation forces in the end-effector of the manipulator which are produced by link forces and linearly varies with the $\| (J_T)^+(J_T^T)^+ \|$. We call this magnitude translational resistivity measure w_{TR} for a manipulator configuration C. From (28), w_{TR} is obtained by using the properties of the pseudo-inverse matrix as:

$$w_{TR}=\sqrt{\det(J_T^T J_T)} \tag{29}$$

where det(.) is the determinant of the matrix (.).

Rotationability was suggested to describe the ability of a manipulator in generating not translational forces but only moments or torques at the end-effector.[25] Also, we express a method for evaluating quantitatively the ability. If only rotational motion of the top plate is generated without any translational motion by the link forces, the following relations are obtained from (25):

$$f_c=J_T^T\,\tau=0 \tag{30}$$

$$m_c=J_R^T\,\tau\neq 0, \quad m_c\in\Re(J_R^T) \tag{31}$$

$$\tau^T\tau=m_c^T(J_R)^+(J_R^T)^+m_c. \tag{32}$$

Equation (32) means that the resulting moments of the top plate forms an ellipsoid in the three-dimensional Euclidean space, whose space lies in the directions of the eigenvectors of the matrix $(J_R)^+(J_R^T)^+$. The volume of the ellipsoid represents the magnitude of the rotational forces in the end-effector of the manipulator which are produced by link forces and linearly varies with the $\| (J_R)^+(J_R^T)^+ \|$. We call this magnitude rotational resistivity measure w_{RR} for a

https://doi.org/10.1017/S0263574799001368 Published online by Cambridge University Press

manipulator configuration C. From (28), $\boldsymbol{w}_{RR}$ is obtained by using the properties of the pseudo-inverse matrix as:

$$\boldsymbol{w}_{RR} = \sqrt{\det(J_R^T J_R)}. \quad (33)$$

In a given singular configuration, two measures have usually the following values: $\boldsymbol{w}_{TR} = 0$ and $\boldsymbol{w}_{RR} = 0$ from the view point of link force and torque.

We have investigated the singular configurations of the 3-PRPS parallel manipulator by using these measures. To this end, the existence of the seven singular configurations is detected as shown in Figure 12 and Table I. One of the singular configurations occurs at which the top platform and the base plate are paralleled and $\alpha = \beta = \gamma = 0°$. Figures 13(a) and (b) show the results of the measures at the configuration. Obviously, $\boldsymbol{w}$ and $\boldsymbol{w}_R$ represent the fact that the configuration is singular as shown in Figure 13(a). However, the results of $\boldsymbol{w}_{TR}$ and $\boldsymbol{w}_{RR}$ of Figure 12(b) suggest a new fact that the translational motion is able to be carried out at the singular configuration, while the rotational motion can not be accomplished. Therefore, the singularity analysis by using $\boldsymbol{w}_{TR}$ and $\boldsymbol{w}_{RR}$ helps to extend the achievable workspace, while the previous method by the manipulability $\boldsymbol{w}$ and the resistivity $\boldsymbol{w}_R$ restricts the whole motion of the manipulator at a given singular configuration.

7. DEVELOPMENT OF THE PROPOSED MECHANISM

We developed a prototype of the proposed mechanism based on the design method described above. The mechanism will be used as a wrist of a robot for the probing task as shown in Figure 14. The probing task requires large workspace, free manipulation, and high capability of resisting applied forces. Considering design tradeoffs among abovely discussed workspace, manipulability, and resistivity, it is decided that ρ would be unity to compromise such considerations. The specification of the designed mechanism are $R = 16$ [mm], $r = 15$ [mm], $S_i = 5$ [mm] and $L_i = 90 \pm 2.5$ [mm] for $i = 1, 2, 3$. In addition, these specifications satisfy the condition of the existence of the forward kinematic solution.

Each joint actuator for the proposed mechanism utilizes the Lorentz force: the force generated by a current-carrying conductor in a static magnetic field as shown in Figure 15. The conductor, a moving coil, is positioned among four rectangular neodyminum iron boron magnets which provide a high gap field. The designed actuator has various features as a fast response, a minimal mass, and a linear force generation.[13] The force constant measured in motion direction of the actuator is 0.8 N/A. These characteristics of the actuator can provide the best potential for the probing task application. The position of the actuator is measured by an optical sensor. This sensor is composed of a diode laser, two mirrors and a PSD (position sensing device). The position sensing resolution of this device is approximately $\pm 5\mu$m. To reflect accurately the applied forces on the links of the mechanism, an one dimensional force sensor is installed at each actuating link. The force sensor provided reading up to 10 N with a resolution of 2.22×10^{-4} N.

8. CONCLUSIONS

We have presented a kinematic analysis of the 3 PRPS type parallel manipulator developed for probing task applications. It was found that the quantity ρ (the ratio of the top plate and the base plate size) is the most influential design parameter.

The forward kinematic solution is not uniquely determined, but the analysis shows that there exist eight distinct solutions according to the initially guessed angles θ_i between the base platform and the vertical links. The existence conditions of such solutions are defined in terms of ρ and link displacements as shown in (16). The ratio ρ is also found to be an important design parameter for determining the workspace volume. As ρ decreases, larger workspace is obtained. The developed manipulator possesses the workspace which forms the shape of the hexagonal pole without changing the sectional area.

Using the translational resistivity $\boldsymbol{w}_{TR}$ and the rotational resistivity $\boldsymbol{w}_{RR}$, we can check the singularity of the manipulator. At a singular configuration of the manipulator, the two measures have usually the following values: $\boldsymbol{w}_{TR} = 0$ and $\boldsymbol{w}_{RR} = 0$ from the view point of link force and torque. The singularity analysis using $\boldsymbol{w}_{TR}$ and $\boldsymbol{w}_{RR}$ helps to extend the achievable workspace when compared with the analysis using the manipulability.

We designed a parallel wrist that has a desired workspace, manipulability, and resistivity for the probing task, and built it as a prototype. Each joint actuator for the proposed mechanism is an electromagnetic linear actuator that has a fast response and a linearized force generation suitable for the probing task. Future research will be directed towards the experimental investigation for active contact control.

References

1. D. Stewart, "A Platform with Six Degree of Freedom" *Proc. Inst. Mech. Eng.* **180**(15), 371–386 (1965).
2. J.P. Merlet, "Force-Feedback Control of Parallel Manipulators" *Proc. of IEEE Int. Conf. on Robotics and Automation* (1988) pp. 1484–1489.
3. Y.K. Byun, D.Y. Kim, and H.S. Cho, "Analysis of a 6-DOF Pose/Wrench Sensor Integrated Stewart Platform-Based Robotic Wrist" *Proc. of '95 ISMCR* (1995) pp. 283–288.
4. X. Geng and L.S. Haynes, "Six-Degree-of-Freedom Active Vibration Isolation Using a Stewart Platform Mechanism" *J. Robotics Systems* **10**(5), 725–744 (1993).
5. C.L. Collins and G.L. Long, "The Singularity of an In-Parallel Hand Controller for Force-Reflected Teleoperation" *IEEE Trans. on Robotics and Automation* **11**(5), 661–669 (1995).
6. F. Behi, "Kinematic Analysis for a Six-Degree-of-Freedom 3-PRPS Parallel Manipulator" *IEEE J. Robotics and Automation* **4**(5), 561–565 (1988).
7. J. Hudgens and D. Tesar, "A Fully-Parallel Six Degree-of-Freedom Micromanipulator: Kinematic Analysis and Dynamic Model" *Proc. 20th Biennial ASME Mechanisms Conf.* (1988) **Vol. 15–3**, pp. 29–38.
8. R.I. Alizade and N.R. Tagiyev, "A Forward and Reverse Displacement Analysis of a 6-DOF In-Parallel Manipulator" *Mech. Mach. Theory* **29**(1), 115–124 (1994).
9. Y.K. Byun and H.S. Cho, "Analysis of a Novel Six-D.O.F. 3-PPSP Parallel Manipulator" *Int. J. Robotics Research* (to appear).
10. A. Sharon, N.N. Hogan, and D.E. Hardt, "High Bandwidth Force Regulation and Inertia Reduction using a Macro/Micro Manipulator System" *Proc. of the IEEE Int. Conf. on Robotics*

https://doi.org/10.1017/S0263574799001368 Published online by Cambridge University Press

and Automation(1988) pp. 126–132.
11. C. Reboulet and R. Pigeyre, "Hybrid Control of A 6-DOF In-Parallel Actuated Micro-Manipulator Mounted on a SCARA Robot" *Int. J. Robotics and Automation* **7**(1), 324–330 (1992).
12. J.H. Shim, H.S. Cho, and S. Kim, "Impact Control of a Probing Manipulator Contacting with Plastically Deformable Environment" *Proc. of the 11th Int. Conf. on Systems Engineering*, Las Vegas (1996) pp. 987–993.
13. J.H. Shim, H.S. Cho and S. Kim, "A New Probing System for the In-Circuit Test of a PCB" *Proc. of the IEEE Int. Conf. on Robotics and Automation*, Minneapolis (1996) pp. 580–585.
14. J.H. Shim, J.Y. Park, D.S. Kwon, H.S. Cho, and S. Kim,"Kinematic Design of a Six Degree-of-Freedom In-Parallel Manipulator for Probing Task" *Proc. of the IEEE Int. Conf. on Robotics and Automation*, Albuquerque (1997) pp. 2967–2973.
15. T. Yoshikawa, *Foundations of Robotics*: *Analysis and Control* (MIT Press, Massachusetts, 1990).
16. R.S. Stoughton and T. Arai, "A Modified Platform Manipulator with Improved Dexterity" *IEEE Trans. on Robotics and Automation* **9**(2), 166–173 (1993).
17. T. Yoshikawa, "Manipulability of Robotic Mechanism" *Int. J. Robotics Research* **4**(2), 3–9 (1985).
18. H. MacCallion and D.T. Pham, "The Analysis of a Six Degree of Freedom Work Station for Mechanized Assembly" *Proc. 5th World Congress on Theory of Machines and Mechanisms* (1979) pp. 611–616.
19. E.F. Fichter, "A Stewart Platform based Manipulator: General Theory and Practical Construction" *Int. J. Robotics Research* **5**(2), 157–181 (1986).
20. G. Gosselin and J. Angeles, "Singularity Analysis of Closed Loop Kinematic Chains" *IEEE Trans. on Robotics and Automation* **6**(3), 281–290 (1990).
21. J.-P. Merlet, "Singular Configurations of Parallel Manipulators and Grassman Geometry" *Int. J. of Robotics Research* **8**(5), 45–56 (1989).
22. G.L. Long and R.P Paul, "Singularity Avoidance and the Control of an Eight-Revolute-Joint Robot Manipulator" *Int. J. Robotics Research* **11**(6), 503–515 (1992).
24. J.Y. Park, "Modeling and Control of a 6-Degree-of-Freedom Micro-Positioning Parallel Manipulator" *M.S. Thesis* (Korea Advanced Institute of Science and Technology, 1996).
25. T. Arai and T. Sheridan, "Characteristics and Mechanism Analysis of Parallel Link Manipulator" *Proc. of IFAC Symposium on Robot Control* (1988) pp. 41.1–41.6.
26. K. Kosuge, M. Okuda, H. Kawamata and T. Fukuda, "Input/Output Force Analysis of Parallel Link Manipulators" *Proc. of IEEE Int. Conf. on Robotics and Automation* (1993) pp. 714–719.

https://doi.org/10.1017/S0263574799001368 Published online by Cambridge University Press